Modeling of Phosphate Removal by Mg-Al Layered Double Hydroxide Functionalized Biochar and Hydrochar from Aqueous Solutions

Azimzadeh, Yaser; Najafi, Nosratollah*[+]; Reyhanitabar, Adel; Oustan, Shahin
Department of Soil Science, Faculty of Agriculture, University of Tabriz, Tabriz, I.R. IRAN

Khataee, Ali Reza
Research Laboratory of Advanced Water and Wastewater Treatment Processes, Department of Applied Chemistry, Faculty of Chemistry, University of Tabriz, Tabriz, I.R. IRAN

ABSTRACT: *Layered double hydroxide functionalized biochar and hydrochar composites are environmentally friendly and low-cost adsorbents for the removal of phosphate from aqueous solutions. In the present study, Mg-Al layered double hydroxide functionalized apple wood biochar and hydrochar were prepared and their phosphate adsorption characteristics were examined through batch experiments. Moreover, important factors affecting adsorption including initial phosphorus concentration (25-200 mg/L), contact time (5-120 min), ionic strength (deionized water, and 0.001, 0.01, and 0.1 mol/L KCl), pH (3-10), and adsorbent dosage (1, 2, 3, and 4 g/L) were investigated. Based on the results, the phosphate adsorption by Mg-Al layered double hydroxide modified biochar and hydrochar were comparable with Mg-Al layered double hydroxide and were greater than biochar and hydrochar. As expected, phosphate adsorption was decreased by increasing solution pH and ionic strength. The highest phosphate removal was attained at pH 4, adsorbent dosage of 4 g/L, and in the presence of deionized water as a background solution. Determination of adsorption characteristics of the adsorbents revealed that the phosphate adsorption mechanism involved a combination of electrostatic attraction, interlayer anion exchange, and formation of surface complexes. The Mg-Al layered double hydroxide modified biochar and hydrochar composites as cost-effective and efficient adsorbents suggest alternative biochar- and hydrochar-based composites for the phosphate removal from contaminated waters that could be used as P-fertilizers.*

KEYWORDS: *Adsorption; Biochar; Composite; Hydrochar; Layered double hydroxide*.

INTRODUCTION

It is generally believed that managing and controlling phosphate levels can be crucial in many ways. In fact, it is a strategic goal of sustainable environmental management to recover phosphorus (P) from aquatic ecosystems using efficient and cost-effective methods and its reuse as a P-fertilizer [1]. A destructive consequence of P delivery

* *To whom correspondence should be addressed.*
+ E-mail: n-najafi@tabrizu.ac.ir ; nanajafi@yahoo.com
1021-9986/2021/2/565-579 15/$/6.05

into surface waters can be eutrophication that starts at dissolved P concentration of 0.02 mg/L. Eutrophication interferes with the natural functions and the structure of aquatic ecosystems, raises water treatment costs, and may help formation of harmful algal blooms [2]. Also, the mine resources of P fertilizers can be exhausted due to over-fertilization. On the other hand, since non-renewable rock phosphate resources are limited, which will make its value go up when not enough P fertilizers are available to ensure future food security [3]. The recovery of lost phosphate protects environmental water quality and improves food security by minimizing supply risks.

Quite many technologies (e.g. biological P uptake, adsorption, and chemical precipitation) have been developed for this purpose among which adsorption is considered as a high-performance method because of its convenience, high selectivity, easy application and no secondary contamination [4]. Several different sorbents such as metal oxides [5], engineered biochar [6], engineered hydrochar [7] and layered materials [8] have been used to eliminate phosphate from contaminated waters. Layered double hydroxides (LDHs) are brucite like octahedral sheets with anion or oxyanions and water molecules in the interlayer space and have high ability to remove anions, especially phosphate from water. The general formula of these layered inorganic compounds can be presented as $\left[M^{2+}_{1-x}M^{3+}_{x}(OH)_2\right]^{x+}\left[A^{n-}_{x/n}.mH_2O\right]^{x-}$, where M^{2+} and M^{3+} are divalent and trivalent cations, respectively. $A^{n-}_{x/n}$ is an interlayer anion with charge n, and x is $M^{3+}/[M^{2+}+M^{3+}]$ ratio where the value of x falls in a range of 0.17 to 0.33 [9]. The content and nature of M^{2+} and M^{3+} cations strongly affect the adsorption capacity of LDHs [10]. Das et al. [10] reported that the LDHs prepared from Mg and Al cations demonstrate a greater adsorption capacity than other LDHs. LDHs have been used for adsorption of phosphate because of their high positive charge, easily exchangeable interlayer anions, and great specific surface area [11]. However, the wide application of LDHs is inhibited because of problems including low renewability, high cost, difficult disposal after using [12], and difficult particle separation [13]. In addition, LDHs in bulk or granular forms have low hydraulic conductivity or high diffusion resistance [13]. Therefore, they are not suitable for filtration systems. However, when the nano-sized adsorbents such as LDHs are attached to larger particles such as biochar or hydrochar, their environmental applications would be highly beneficial [9]. Also, these composites have agricultural and environmental advantages such as soil fertility improvement and carbon sequestration.

Biochar is a pyrogenic recalcitrant porous material produced from biomass heating in an oxygen-limited medium. Hydrochar is an energy-dense solid produced Through Hydrothermal Carbonization (HTC). Biochar and hydrochar have a great potential for carbon sequestration and have been employed as soil conditioners or stable adsorbents because of their stable porous structures, oxygen-containing functional groups and easy to produce and use [14]. *Xiao et al.* [15] interpreted the biochars applications such as adsorbents, fertilizers and carbon fixators. Also, *Lian* and *Xing* [16] reviewed the morphology, fractions and molecular structure of biochar and the role of biochar physicochemical properties in its stability and sorption behavior. Advantageous properties and features such as stable carbon matrix, environmentally friendly, low cost, high porosity, high specific surface area, and easy preparation and operation qualify biochar and hydrochar as matrix for stabilizing LDH flakes and creating LDH-biochar and LDH-hydrochar composites. Hence, some novel composites from biochar, hydrochar and LDHs nanoparticles have lately been prepared for adsorption of phosphate [17-19], nitrate [20], and arsenic [9]. For instance, *Li et al.* [18] and *Wan et al.* [19] prepared a Mg/Al-LDH modified biochar by immersing a biochar produced from sugarcane leaves and bamboo in $MgCl_2$ and $AlCl_3$ solution at pH 10. *Tan et al.* [21] synthesized the LDH flakes on biomass and then prepared a LDH-biochar by pyrolyzing the LDH pre-coated biomass. These engineered biochars proved to offer a high removal potential for anions from aqueous solutions. *Wan et al.* [19] revealed that the P-loaded LDH-biochar had potential application as a slow-release P-fertilizer without application of any chemical P-fertilizer. Therefore, these novel adsorbents can be used for removal of P from contaminated waters and potentially can be used as slow release P-fertilizers for surmounting the eutrophication of water resources as well as exhaustion of P resources challenges. The adsorption conditions such as ionic strength, pH, and adsorbent dosage, are associated with adsorption mechanisms and could affect the adsorption capacity of the adsorbents.

Many researchers have investigated the effects of ionic strength, pH, and adsorbent dosage on phosphate adsorption with different adsorbents [22,23]; nevertheless, there is notably not a wealth of literature on adsorption characteristics of LDH-biochar and specially LDH-hydrochar composites for the phosphate. Such an investigation can offer insights and provide information on how to produce high-efficiency LDH-biochar and LDH-hydrochar composites involved in development of biochar and hydrochar technologies. The present study in addressing such a gap employs self-assembly co-precipitation method in order to prepare Mg/Al-LDH-biochar (LDH-biochar) and Mg/Al-LDH-hydrochar (LDH-hydrochar) composites for phosphate removal from aqueous mediums.

EXPERIMENTAL SECTION

Materials

Analytical grades $AlCl_3.6H_2O$, $MgCl_2.6H_2O$, NaOH, and $KH_2PO_4.H_2O$ were purchased from Merck Company, Germany. The wood feedstock for producing biochar and hydrochar was obtained from pruned parts of an apple orchard in Miandoab, West Azerbaijan Province, Iran. The apple wood was chipped into 2 mm pieces, then was oven dried overnight at 80 °C after washing with deionized water.

Adsorbent production and preparation

Biochar was produced via slow pyrolysis of apple wood feedstock at 600 °C for 1 h in the presence of Argon (Ar) gas flow [9]. Hydrochar was produced *via* hydrothermal carbonization (HTC) of apple wood feedstuck at 180 °C for 12 h [7]. The prepared biochar and hydrochar were then ground to attain 0.5-1.0 mm size particles in order to eliminate the residual ash [24]. After being washed with deionized water, they were immediately oven-dried overnight at 105 °C before use [18].

LDH-biochar and LDH-hydrochar composites were manufactured by co-precipitating mixed solutions of $MgCl_2.6H_2O$ and $AlCl_3.6H_2O$ [17,18,19]. In fact, 10 g biochar or hydrochar was added to 100 mL of a solution containing 0.03 mole of $MgCl_2$ and 0.01 mole of $AlCl_3$ under stirring. Subsequently, the pH of the mixture was setted to 10 with 1.0 M NaOH solution. The obtained dispersion was aged in a sealed bottle at 80 °C for 3 days, and oven dried overnight at 80 °C after washing with deionized water. Finally, the synthesized composites were ground to attain 0.5-1.0 mm size particles.

For synthesizing of the LDH particles, a solution containing $AlCl_3.6H_2O$ and $MgCl_2.6H_2O$ with a Mg/Al molar ratio of 3 was added into NaOH solution within a few seconds under stirring and N_2 purging. Then separated and washed with deionized water in several rounds. The aqueous dispersion was then hydrothermally treated in an HTC reactor at 180 °C for 24 h [25], and finally dried, ground and sieved to 0.5-1.0 mm diameter range.

Characterizations

The surface morphological characteristics of LDH, LDH-biochar, and LDH-hydrochar were analyzed employing a scanning electron microscopy (MIRA3-FEG-SEM). The X-Ray Diffraction (XRD) analysis was performed using a PW1730 X-ray diffractometer (Philips Electronic Instruments), with CuKα radiation (λ=0.15419 nm) over a 2θ range of 5-70°. The XRD results were analyzed by X'Pert highscore software. Using these analytical tools have also been reported in characterizing similar composites in the literature [17,18]. The specific surface area (S_{BET} values), mean pore diameter (MPD values) and total pore volume (TPV values) of biochar, hydrochar, LDH, LDH-biochar, and LDH-hydrochar samples were measured using a BELsorp- mini II analyzer (BEL Japan Inc., Osaka, Japan). To determine the pH and EC, 1g of each biochar, hydrochar or the adsorbents mixed with 10 mL of deionized water was shaken on a mechanical shaker for 2 h and then measured with a pH meter (HANNA, pH 209, Italy) and EC meter (RS232 Conductivity/TDS meter 8301, Taiwan), respectively [14]. Point of Zero Charge (PZC) of the LDH, LDH-biochar, and LDH-hydrochar was determined using 0.1 and 0.01 M NaCl solutions and 1 g/L adsorbent suspensions (pH adjusted between 6 and 13 by 0.1 M NaOH and 0.1 M HCl) [26].

Batch adsorption experiments

The phosphate standard solutions were prepared in 0.03 mol/L KCl solution using KH_2PO_4. Adsorption experiments were performed under following conditions: time intervals of 5-120 min, phosphate initial concentration range of 25–200 mg/L, ionic strength (deionized water and 0.001-0.1 mol/L KCl), pH of 3–10, adsorbent dosage of 1–4 g/L, and at room temperature (22.0 ± 0.5 °C). 0.1 mol/L solutions of KOH or HCl were used to adjust the solution pH. All experiments were carried out in triplicate.

For the kinetic experiments, 0.1 g of adsorbent was added into a set of 100 mL Erlenmeyer flask containing 50 mL of 0.03 mol/L KCl solution with P concentration of 50 mg/L. The flasks were shaked on a shaker (at 170 rpm) for different times (5-120 min). Then, the flasks were picked up and the dispersions were filtered by a microsyringe (0.22 µm). To determine the phosphate concentration of the filtrate at a wavelength of 880 nm, a Philler Scientific SU6100 spectrophotometer (USA) was employed. The amount of P adsorbed by the adsorbents (q_e, mg/g) was calculated using the Equation 1.

$$q_e = \frac{V(C_i - C_e)}{m} \quad (1)$$

In which, *V* (L) is the volume of phosphate solution, *m* (g) represents the adsorbent mass, C_i and C_e (mg/L) are the initial and equilibrium concentrations of phosphate, respectively.

The kinetics data of P adsorbed on LDH, LDH-biochar, and LDH-hydrochar were fitted with Pseudo-first- (Eq. (2)), pseudo-second-order (Eq. (3)), Elovich (Eq. (4)), and intra-particle diffusion (Eq. (5)) models [27]:

$$q_t = q_e\left(1 - e^{-k_1 t}\right) \quad \text{First-order model} \quad (2)$$

$$q_t = \frac{k_2 q_e^2 t}{1 + k_2 q_e t} \quad \text{Second-order model} \quad (3)$$

$$q_t = \left(\frac{1}{\beta}\right)\ln(\alpha\beta) + \left(\frac{1}{\beta}\right)\ln t \quad \text{Elovich model} \quad (4)$$

$$q_t = K_{dif} t^{0.5} + C \quad \text{Intra-particle diffusion mod} \quad (5)$$

In which, q_e and q_t (mg/g) represent the amount of phosphate adsorbed at equilibrium time and at time *t*, respectively; k_1 (1/min) and k_2 (g/mg min) are the rate constants of the adsorption, α (mg/mL min) is the initial adsorption rate constant, β (mL/mg) is related to the activation energy for chemisorption, K_{dif} (mg/mL $min^{0.5}$) is the intra-particle diffusion rate constant of, and *C* (intercept) represents the boundary layer effect [28].

Isotherm experiments were performed through adding 0.1 g of adsorbents to a set of 100 mL Erlenmeyer flask containing 50 mL of 0.03 mol/L KCl solution with a P concentration range of 25-200 mg/L. The flasks were shaked on a rotary shaker (at 170 rpm). After 2 h, dispersions were filtered by a microsyringe (0.22 µm) and phosphate concentration was determined as described above. Freundlich and Langmuir isotherm models were used to describe the P adsorption process on LDH, LDH-biochar, and LDH-hydrochar [7,18]:

$$q_e = K_F C_e^{\frac{1}{n}} \quad \text{Freundlich} \quad (6)$$

$$q_e = \frac{b K_L C_e}{1 + K_L C_e} \quad \text{Langmuir} \quad (7)$$

where, K_F ($mg^{(1-n)}$ L^n/g) and n are the affinity constant and the linearity constant of Freundlich model, respectively, K_L (L/mg) and b (mg/g) are the bonding coefficient and maximum adsorption capacity of Langmuir model, and C_e (mg/L) denotes the equilibrium concentration of the adsorbate [18].

The Freundlich isothermal model depicts the non-ideal adsorption on heterogeneous surfaces. Instead, the Langmuir adsorption isothermal model assumes the monolayer adsorption onto homogeneous surfaces, without any interactions between the adsorbed molecules [29].

To explore the pH effect on the adsorption process, 0.1 g of adsorbent was loaded in a 100 mL Erlenmeyer flask containing 50 mL of 0.03 mol/L KCl solution with P concentration of 50 mg/L and was thoroughly mixed. Following that adjusting the pH of dispersions at 3, 4, 5, 6, 7, 8, 9 and 10 by 0.1 mol/L KOH and HCl solutions was done. After being shaken for 2 h, the solution's pH of dispersions was determined using a pH meter (HANNA, pH 209) and the P concentration of the filtrates was measured.

To test the ionic strength influence, 0.1 g of adsorbent was loaded in a 100 mL Erlenmeyer flask containing 50 mL of deionized water, 0.001, 0.01 and 0.1 mol/L KCl solution with P concentration of 50 mg/L at pH 4. After shaking for 2 h, the P concentration of the filtrate was measured.

To test the adsorbent dosage influence, 0.05, 0.1, 0.15 and 0.2 g of adsorbent were loaded in a 100 mL Erlenmeyer flask containing 50 mL of 0.03 mol/L KCl solution with P concentration of 50 mg/L at pH 4. The P concentration of the filtrates was measured after shaking for 2 h.

Statistics

All adsorption experiments were conducted with three replicates. Data analysis (the two-sample t-test) was performed by SPSS, Version 21 software. All kinetics and

isothermal data were fitted using GraphPad Prizm (Version 6.07) software, and the standard error of estimate (SEE) and determination coefficient (r^2) values of the fitted equations were determined. The SEE for determination of the goodness of data fit to the models was calculated as follows [30]:

$$SEE = \left[\frac{\sum (q_e - q_e^*)^2}{(n-2)} \right]^{0.5} \quad (8)$$

Where n is the number of measurements and q_e and q_e^* are the amount of P adsorption (mg/g) measured by the experiment and predicted by the models, respectively.

RESULTS AND DISCUSSION

Characterization analysis

A number of physical properties of the biochar, hydrochar, LDH, LDH-biochar, and LDH-hydrochar samples were presented in the Table 1. The specific surface area (S_{BET} values) and total pore volume (TPV) values of the LDH-biochar and LDH-hydrochar composites increased as compared with the biochar and hydrochar alone. The S_{BET} value of the synthesized LDH-biochar and LDH-hydrochar were found to be 40.94 and 26.21 m^2/g, respectively (Table 1). A similar result for LDH-biochar was reported by *Wan et al.* [19], who obtained the value of 44.6 m^2/g, while *Li et al.* [18] reported the value of 11.41 m^2/g. These differences may be related to the differences of biochar properties and synthesis methods.

The higher TPV of LDH-biochar and LDH-hydrochar than the biochar and hydrochar alone may have been caused by deposition of LDH particles on the outer surfaces of the biochar and hydrochar, and the lower mean pore diameter (MPD) of LDH-biochar may be attributed to deposition of LDH particles on the inner surfaces of biochar. Also, the presence of LDH particles on the biochar and hydrochar increased the LDH-biochar and LDH-hydrochar specific surface area even more than the LDH [7]. These results were further supported by the SEM images of LDH-biochar and LDH-hydrochar (Fig. 2). These results confirmed the capability of biochar and hydrochar as matrix to stabilize LDH particles. The PZC for the LDH, LDH-biochar and LDH-hydrochar was determined about 12.1, 10 and 9.8, respectively. *Halajnia et al.* [29] reported 12.5 for the PZC of Mg/Al-LDH. The pH of the LDH was 9.16 and the pH of the LDH-biochar and LDH-hydrochar was lower than that of the LDH (Table 1), that may be related to the lower content of the LDH particles in the composites structure. According to *Goh et al.* [35], the natural pH of LDH suspension was 9.5.

The amounts of initial materials used to produce 100 g of LDH, LDH-biochar and LDH-hydrochar were shown in the Table 2. The sum of used Mg and Al salts to produce 100 g of LDH, LDH-biochar, and LDH-hydrochar were 162.6, 59.3, and 68.0 g, respectively. In addition, the yields (weight percentage) of obtained LDH-biochar and LDH-hydrochar per mass of the materials used ($MgCl_2.6H_2O$ and $AlCl_3.6H_2O$, NaOH, biochar and hydrochar) were 65.7% and 56.7%, while this value was 46.8% for the LDH. Therefore, the LDH-biochar and LDH-hydrochar were more cost-effective than the LDH because of higher yields and lower consumption of the Mg and Al salts.

XRD

A series of intense and sharp symmetric diffraction peaks were detected in the XRD patterns of the adsorbents in the 2θ range of 5–70°, which were shown in the Fig. 1. All XRD patterns (except for biochar and hydrochar) resembled the normal XRD pattern of a hydrotalcite mineral [31]. The diffraction peaks of LDH-biochar and LDH-hydrochar composites confirmed the formation of LDH particles on the biochar and hydrochar surfaces [18]. These results were in line with other studies [17,18]. The location of the detected peaks and its similarity to the LDHs compounds indicated the crystal structure of the prepared LDH-biochar and LDH-hydrochar composites [18]. The absence of any other characteristic peaks could verify the fact that the LDH-biochar and LDH-hydrochar were composite of LDH with biochar or hydrochar [32].

The presence of 012, 015, 018 and 110 peaks exhibited a hexagonal lattice with rhombohedral 3R symmetry [33]. The interlayer d-space values (d_{003} and d_{006}) were found to be 8.00 and 3.92 Å for the LDH, while the corresponding values were 7.83 and 3.90 Å for the LDH-biochar, and 7.61 and 3.97 Å for the LDH-hydrochar, respectively. The intensity of 003 reflection was about twice as much as 006, which indicated a favorable layer structure for the adsorbents [31]. The crystallographic parameter (α) of the LDH, LDH-biochar, and LDH-hydrochar calculated from diffraction peak of 110 [34] turned out to be 0.306 nm. These values indicated that the LDH-biochar and LDH-

Table 1: Physical and chemical characteristics of the biochar, hydrochar, LDH, LDH-biochar and LDH-hydrochar.

Adsorbent	S_{BET} (m^2/g)	TPV (cm^3/g)	MPD (nm)	pH	EC (dS/m)	PZC
Biochar	1.05	0.0048	18.42	9.52	0.19	-
Hydrochar	2.61	0.0066	10.12	5.81	0.08	-
LDH	24.82	0.2074	33.42	9.16	0.70	12.1
LDH-Biochar	40.94	0.1667	0.16	8.81	0.58	10.0
LDH-Hydrochar	26.21	0.1002	15.29	8.46	0.62	9.8

TPV: Total pore volume (p/p_0=0.99); MPD: mean pore diameter; S_{BET}: specific surface area; PZC: point of zero charge

Table 2: Initial materials used for producing 100 g of LDH, LDH-biochar and LDH-hydrochar.

Adsorbent	Initial materials	Amount (g)	Yield (%)
LDH-Biochar	$MgCl_2.6H_2O$	42.5	100×100/152.1 =65.7
	$AlCl_3.6H_2O$	16.8	
	NaOH	23.2	
	Biochar	69.6	
	Total	152.1	
LDH-Hydrochar	$MgCl_2.6H_2O$	48.7	100×100/176.3 =56.7
	$AlCl_3.6H_2O$	19.3	
	NaOH	28.4	
	Hydrochar	79.9	
	Total	176.3	
LDH	$MgCl_2.6H_2O$	116.5	100×100/213.5 =46.8
	$AlCl_3.6H_2O$	46.1	
	NaOH	50.9	
	Total	213.5	

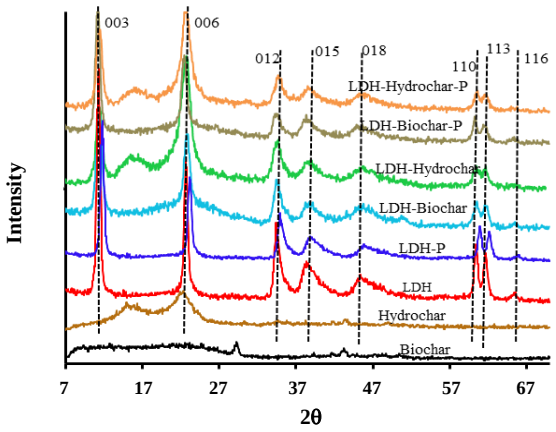

Fig. 1: XRD patterns of the LDH, LDH-biochar, and LDH-hydrochar before and after P adsorption.

hydrochar composites were created successfully employing the co-precipitation method [17].

The similarity of XRD patterns of the studied adsorbents (LDH, LDH-biochar and LDH-hydrochar) before and after P adsorption suggested that P adsorption was not along with the formation of Mg-P minerals such as $MgHPO_4$ and $Mg(H_2PO_4)_2$ crystals on the surface of adsorbent which Yao et al. [6] detected in the surface of MgO-biochar composite after P adsorption. However, the intensity of the diffraction peaks was decreased after P adsorption on the all adsorbents (Fig. 1), probably due to the exchange of phosphate with inter layer chloride [19].

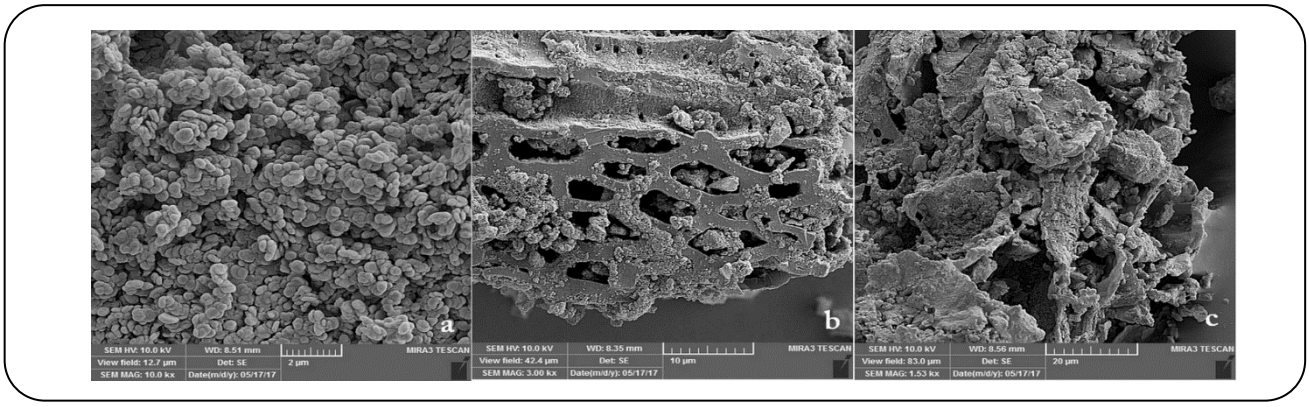

Fig. 2: The SEM images of the LDH (a), LDH-biochar (b), and LDH-hydrochar (c).

SEM analysis

The surface morphological features of the LDH, LDH-biochar and LDH-hydrochar were shown in the Fig. 2. The hexagonal flakes were observed in SEM images of LDH (Fig. 2a). The presence of LDH particles on the biochar and hydrochar surfaces was observed clearly (Fig. 2b and c). The LDH-biochar and LDH-hydrochar surfaces and pores were covered and filled with fine LDH particles (Fig. 2b and c). The morphology of the LDH-biochar and LDH-hydrochar composites were porous, fuzzy and rough due to the biochar and hydrochar nature (Fig. 2b and c).

Batch experiments

Adsorption kinetics

The P adsorption kinetics on the LDH, LDH-biochar, and LDH-hydrochar was initially fast and then proceeded slowly until reached equilibrium at 30, 60, and 30 min, respectively (Fig. 3). The similar results for P adsorption onto LDH-biochar composite [19] and LDH [8] have already been reported. The adsorption rate of phosphate by LDH-biochar was lower than the LDH and LDH-hydrochar that may be related to heterogeneity of the LDH-biochar surface [4,35]. The LDH, LDH-biochar, and LDH-hydrochar removed more than 89%, 83%, and 84% of solution phosphate at the equilibrium time, respectively. However, the two-sample t-test revealed that there were no significant differences between P adsorption on the LDH, LDH-biochar, and LDH-hydrochar irrespective of the contact time. The adsorption rates of the LDH, LDH-biochar, and LDH-hydrochar composites were much higher than previously reported LDHs and engineered biochars and hydrochars [7, 24]. Yao et al. [36] showed that the P adsorption on biochars synthesized through slow pyrolysis of tomato leaves reached equilibrium after 24 h. However, *Li et al.* [18] and *Wan et al.* [19] reported that P adsorption on the LDH-biochar composite reached equilibrium at less than 1 h. Therefore, the presence of nano-LDH particles on the biochar and specially hydrochar surfaces could accelerate the P adsorption process.

The kinetic parameters of P adsorption on the LDH, LDH-biochar and LDH-hydrochar were shown in the Table 3. The Elovich and pseudo-first- and pseudo-second-order kinetics models could duly account for the adsorption data, indicating the coexistence of multiple mechanisms in adsorption of P on the LDH, LDH-biochar, and LDH-hydrochar. However, higher r^2 and lower SEE of the pseudo-second-order model in comparison with the pseudo-first-order model indicated that the phosphate adsorption process was predominantly controlled by chemical interactions [37]. In addition, the maximum adsorption capacities obtained from the pseudo-second-order model were close to the experimental results (Table 3).

It has previously been shown that the kinetics data of phosphate adsorption on the LDHs, LDH-biochar, and LDH-hydrochar could be best described by the pseudo-first- and pseudo-second-order kinetic models but the data could be better fitted to the pseudo-second-order kinetic model [7,8,18,19]. The k_1 and k_2 pertain to the P adsorption power of adsorbents. The k_2 values of the LDH, LDH-biochar, and LDH-hydrochar were 0.021, 0.026, and 0.028 g/mg min, respectively, which were found to be much greater than that of biochar (0.0005 g/mg min) [36]. The k_1 values of the LDH, LDH-biochar, and LDH-hydrochar were 0.245, 0.274, and 0.279 1/min, respectively which were about hundred times greater than that of biochar (0.0026 1/min) [24]. The α values of LDH, LDH-biochar,

Table 3: The kinetic model parameters for phosphate adsorption simulation.

Adsorbent	q_{max*} (mg/g)	Pseudo-first-order				Pseudo-second-order				Elovich			
		q_e (mg/g)	k_1 (1/min)	r^2	SEE	q_e (mg/g)	k_2 (g/mg min)	r^2	SEE	α (mg/mL min)	β (mL/mg)	r^2	SEE
LDH	22.26	21.54	0.245	0.811	1.006	22.76	0.021	0.972	0.387	6337	0.561	0.849	0.899
LDH-biochar	21.09	20.38	0.274	0.815	0.836	21.45	0.026	0.993	0.166	22452	0.661	0.871	0.698
LDH-hydrochar	21.04	20.51	0.279	0.847	0.737	21.51	0.028	0.981	0.259	55310	0.705	0.813	0.814

** The maximum P adsorption in 50 mg P/L solution*

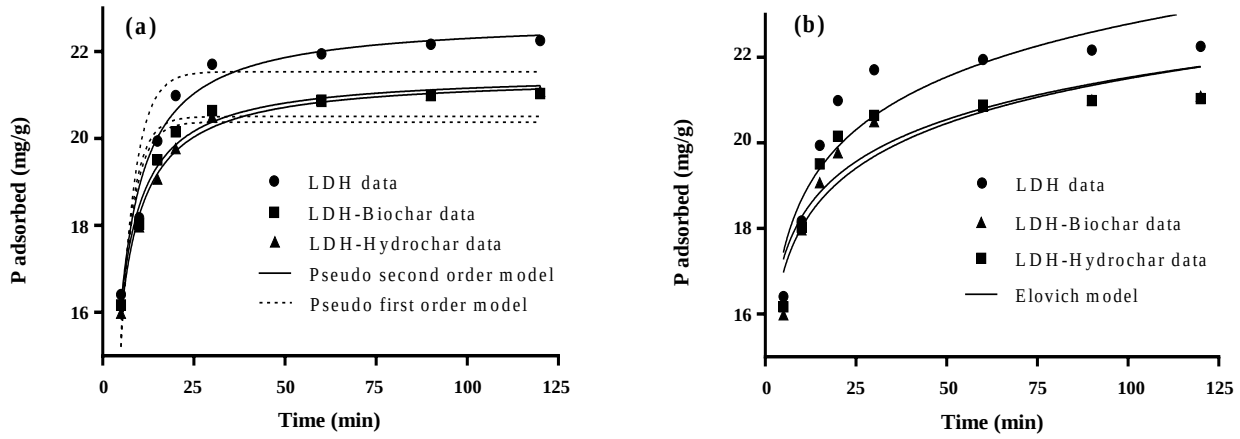

Fig. 3: Kinetics of phosphate adsorption on the LDH, LDH-biochar, and LDH-hydrochar (P concentration = 50 mg/L, pH = 4, adsorbent dosage = 2 g/L, I = 0.03 mol/L KCl at 22 ˚C).

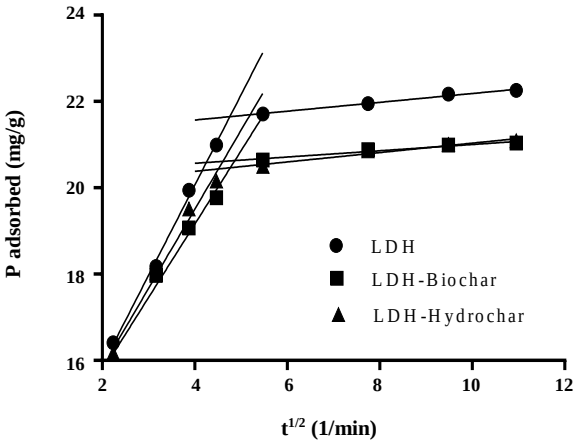

Fig. 4: The plots of intra-particle diffusion model for the adsorption of P onto the LDH, LDH-biochar, and LDH-hydrochar (P concentration = 50 mg/L, pH = 4, adsorbent dosage = 2 g/L, I = 0.03 mol/L KCl at 22 ˚C).

and LDH-hydrochar were 6337, 22452, and 55310 mg/mL min, respectively, and the β values of the adsorbents were 0.561, 0.871, and 0.705 mL/mg, respectively (Table 3).

The relationship between $t^{1/2}$ and q_t was shown in the Fig. 4. The relationship between $t^{1/2}$ and q_t was not linear within the whole adsorption time for all adsorbents suggesting that the intra-particle diffusion model was not capable of expressing the P adsorption kinetics within the whole adsorption time. However, each data set could be divided into two phases with r^2 more than 0.94 (Table 4), indicating that the intra-particle diffusion occurs within the related adsorption period. The first part of the plot obtained for each adsorbent may be related to external surface adsorption and the second part may refer to the intra-particle diffusion [37]. The intra-particle diffusion was not the only operative mechanism because of every line was not passing through the origin (Fig. 4).

Adsorption isotherms

The Freundlich and Langmuir isotherm models were used to fit the batch data of P adsorption on LDH, LDH-biochar, and LDH-hydrochar and the results were summarized in Fig. 5. Also, the parameters of the fitted models were shown in the Table 5. The adsorption

Table 2: Constants and correlation coefficients of intra-particle diffusion model for phosphate adsorption on the LDH, LDH-biochar, and LDH-hydrochar.

Adsorbent	Phase 1				Phase 2			
	K_{dif} (mg/mL $min^{0.5}$)	C	r^2	SEE	K_{dif} (mg/mL $min^{0.5}$)	C	r^2	SEE
LDH	2.091	11.7	0.996	0.148	0.102	21.2	0.987	0.034
LDH-biochar	1.700	12.4	0.983	0.263	0.109	20.0	0.954	0.069
LDH-hydrochar	1.831	12.2	0.988	0.240	0.072	20.28	0.945	0.051

Table 5: Freundlich and Langmuir model parameters calculated for phosphate adsorption.

Adsorbent	Freundlich				Langmuir			
	K_f ($mg^{(1-n)}L^n/g$)	1/n	r^2	SEE	b (mg/g)	K_L (L/mg)	r^2	SEE
LDH	14.82	0.313	0.959	4.582	61.3	0.119	0.998	0.982
LDH-biochar	12.71	0.314	0.957	4.253	55.6	0.098	0.994	1.578
LDH-hydrochar	12.22	0.304	0.956	4.0	51.71	0.096	0.993	1.581

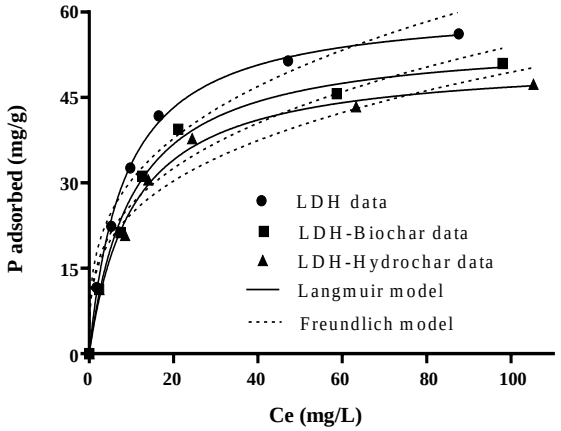

Fig. 5: Fitting Freundlich and Langmuir isotherm models to data of phosphate adsorption by LDH, LDH-biochar, and LDH-hydrochar (pH = 4, adsorbent dosage = 2 g/L, I = 0.03 mol/L KCl at 22 °C).

of phosphate by the adsorbents was described by the Langmuir model better than the Freundlich model. The maximum P adsorption capacities of the LDH, LDH-biochar, and LDH-hydrochar calculated by the Langmuir model (*b*) were 61.3, 55.6, and 51.7 mg/g, respectively. However, the two-sample t-test showed that there were no significant differences between P adsorption on the LDH, LDH-biochar and LDH-hydrochar.

The maximum P adsorption capacities of the oak wood biochar and municipal wastes hydrochar were reported as 3.6 and 5.1 mg/g, respectively [38]. Also, the present study showed that the phosphate adsorption capacities of biochar and hydrochar were 0.45 and 0.16 mg/g in initial P concentration of 50 mg/L while those of LDH, LDH-biochar, and LDH-hydrochar were 22.38, 21.30, and 20.75 mg/g, respectively. So, the phosphate adsorption capacities of the biochar and hydrochar were negligible as compared with the LDH-biochar and LDH-hydrochar composites. In addition, compared with the previous reports for different adsorbents [18,32,39], the LDH, LDH-biochar, and LDH-hydrochar showed greater phosphate adsorption capacity. Therefore, functionalizing of the biochar and hydrochar surfaces with LDH particles dramatically enhanced the P adsorption capacities of the biochar and hydrochar. The amounts of Mg and Al salts used to producing a definite mass of LDH-biochar and LDH-hydrochar were lesser than LDH. In addition, means comparison by t-test showed that the P removal efficiency of the LDH-biochar and LDH-hydrochar were similar to that of the LDH. So, utilizing the LDH-biochar and LDH-hydrochar for purification of phosphate-contaminated waters appears to be more cost-effective than the LDH. In addition, the high adsorption capacity of the LDH-biochar and LDH-hydrochar suggests the spent composites have potential application as P-fertilizers.

The K_L values of the LDH, LDH-biochar, and LDH-hydrochar were 0.119, 0.098, 0.096 L/mg, respectively (Table 5). The higher K_L value shows the higher adsorption ability of adsorbent in low P concentrations [40]. The *n* value in the Freundlich isothermal model denotes

Table 6: Comparison of maximum adsorption capacity of various adsorbents.

Adsorbent	T °C	pH	Dosage (g/L)	Isotherm	Kinetics	q_m (mg/g)	Ref.
Mg/Al-LDH-biochar	25	3.0	2.5	Langmuir	Pseudo-second-order	53.4	[18]
Fe_3O_4@Zn-Al-LDH	25	3.0	2.0	Langmuir	Pseudo-second-order	36.9	[32]
Fe_3O_4@Mg-Al-LDH	25	3.0	2.0	Langmuir	Pseudo-second-order	31.7	
Fe_3O_4@Ni-Al-LDH	25	3.0	2.0	Langmuir	Pseudo-second-order	26.5	
Mg/Fe-LDH	25	8.4	5.0	Langmuir	-	15.5	[39]
Ca/Fe-LDH	25	8.4	5.0	Langmuir	-	28.8	
Calcined (500 °C) Mg/Al-LDH	30	6.0	0.4	Langmuir	Pseudo-first-order	44.3	[10]
Mg/Al-LDH	25	4.0	2.0	Langmuir	Pseudo-second-order	61.3	This work
Mg/Al-LDH-biochar	25	4.0	2.0	Langmuir	Pseudo-second-order	55.6	This work
Mg/Al-LDH-hydrochar	25	4.0	2.0	Langmuir	Pseudo-second-order	51.7	This work

the heterogeneity of the site energies and according to the Freundlich theory, the adsorption isotherm becomes favorable when n < 1, unfavorable when n > 1, and linear when n = 1 [27]. The *n* values of the LDH, LDH-biochar, and LDH-hydrochar were obtained as 3.19, 3.18 and 3.29, respectively. The K_F values of the LDH, LDH-biochar, and LDH-hydrochar were 14.82, 12.71, and 12.22 $mg^{(1-n)}$ L^n/g, respectively. The K_F constant represents the adsorption capacity of adsorbent. The high values of K_F indicate high adsorption capacity [29].

Approximately the same values of r^2 for two models confirmed that the phosphate adsorption process on the LDH, LDH-biochar and LDH-hydrochar was controlled by multiple processes (Table 5). The similar results have also been reported by some previous researchers [8,18].

The Table 6 presents a comparison of phosphate adsorption capacity values for different synthetic adsorbents. The phosphate adsorption capacities obtained for the LDH, LDH-biochar, and LDH-hydrochar composites in this study were greater than many of the similar adsorbents reported in literatures (Table 6).

The powdered LDHs are not favorable materials to be used as an adsorbent in practical applications because of various problems [12,13]. In addition, synthesis of LDH-biochar and LDH-hydrochar required lower amounts of Mg and Al salts than LDHs, which make it more cost-effective [19]. Therefore, the LDH-biochar and LDH-hydrochar seem to be more favorable adsorbents than the LDH, biochar, and hydrochar in waste water purifications [13,19].

Effect of pH

The P adsorption on the LDH, LDH-biochar, and LDH-hydrochar was significantly affected by initial solution pH (pH_i) and the adsorbed phosphate decreased with increasing pH from 3.0 to 10 (Fig. 6a). The ideal pH for LDH, LDH-biochar, and LDH-hydrochar was 4.0. The similar results have also been reported for P adsorption on other similar adsorbents [18,37]. Krishnan and Haridas [41] reported that the optimum pH to reach the maximum adsorption of phosphate by coir pith was 3.0. They explained that different pH values may change relatively dominant phosphate species in solution and anions tendency onto the adsorbent sites. In general, the HPO_4^{2-} and $H_2PO_4^-$ are the dominant P species in the pH range of 3–10, but the concentration of $H_2PO_4^-$ decreases with increasing solution pH. The $H_2PO_4^-$ is more easily adsorbed on the adsorbent surface because of a lower adsorption free energy than HPO_4^{2-} [41]. On the other hand, protonation of adsorbent surfaces at pH values lower than zero point charge (pH_{zpc}) leaves more positively charged surfaces, which increases the adsorption of phosphate anions on LDH particles.

Increasing electrostatic repulsion between more negatively charged surface sites and phosphate anions at pH values above pH_{zpc}, leads to lower phosphate adsorption. In addition, the competitions between phosphate species and OH^- ions at higher pH values would also reduce the adsorption of phosphate by the adsorbent [18]. The initial solution pH had slightly more effect on the LDH-biochar and LDH-hydrochar than LDH because

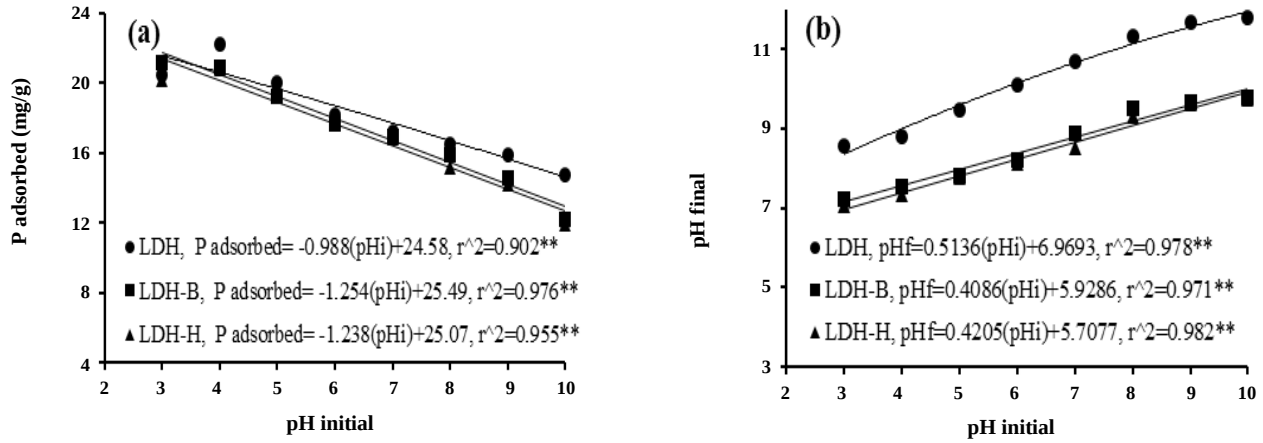

Fig. 6: Negative correlation of phosphate adsorption with solution pH (a) and the effect of initial solution pH on the equilibrium (final) solution pH (b) (P concentration = 50 mg/L, adsorbent dosage = 2 g/L, I = 0.03 mol/L KCl at 22 °C).

of slightly more slope of their regression lines (Fig. 6a). This may be due to the slightly more pH buffering capacity of LDH-biochar and LDH-hydrochar (Fig. 6b). This could be related to the presence of organic matter in LDH-biochar and LDH-hydrochar composites. However, means comparison by t-test for paired samples revealed that no significant differences were observed between P adsorption on the LDH, LDH-biochar and LDH-hydrochar regardless the pH levels.

Linear regression models were significantly fitted ($r>0.90^{**}$) to P adsorption (mg/g) and final solution pH (pH_f) in different initial solution pH levels (Fig. 6a and b). These relationships can be used to forecast the P loading on the adsorbents and final solution pH in different pH values. It was found that for LDH, LDH-biochar, and LDH-hydrochar the equilibrium pH (final pH) was generally higher than the initial pH (Fig. 6b). This could be explained by the acid-base properties of the LDH functional groups, which caused the protonation or deprotonation process [18]. The protonation due to creating more positively charged surface is in favor of phosphate adsorption. Higher equilibrium pH than initial pH concerns the release of the adsorbent hydroxyl groups into the solution [5]. Several studies have shown that higher final pH is due to the partial dissolution of LDHs [10,39]. Thus, the increase in pH after adsorption of phosphate may indicate that the P adsorption on the LDH, LDH-biochar, and LDH-hydrochar may be mainly controlled by chemical interactions.

Effect of ionic strength

The ionic strength (IS) of the solution could influence the adsorption process through affecting the adsorbate activity and adsorbate Diffuse Double Layer (DDL) thickness [35]. The adsorption of phosphate on the LDH, LDH-biochar, and LDH-hydrochar depended on the solution ionic strength (Fig. 7). This may explain the reason why electrostatic mechanisms such as ion exchange play a significant role in the phosphate adsorption on the LDH, LDH-biochar and LDH-hydrochar [35].

Ion exchange is one of the main electrostatic mechanisms of phosphate adsorption on the LDHs. Increasing ionic strength leads to a decrease in activity coefficient of phosphate ions, and eventually P adsorption [22]. However, the phosphate removal percentage with LDH, LDH-biochar, and LDH-hydrochar at 0.1 M KCl was considerable (86%, 79%, and 76%, respectively). This confirms the higher binding affinity of phosphate ions over chloride ions for active sites. The similar results have been reported by previous studies [11,35,42]. Also, the less important effect of ionic strength on the P adsorption by LDH compared to that by LDH-biochar and LDH-hydrochar could explain that the role of electrostatic mechanisms on P adsorption by LDH was less important than by the LDH-biochar and LDH-hydrochar. Means comparison by t-test revealed that there were no significant differences between P removal efficiency of the LDH, LDH-biochar and LDH-hydrochar irrespective

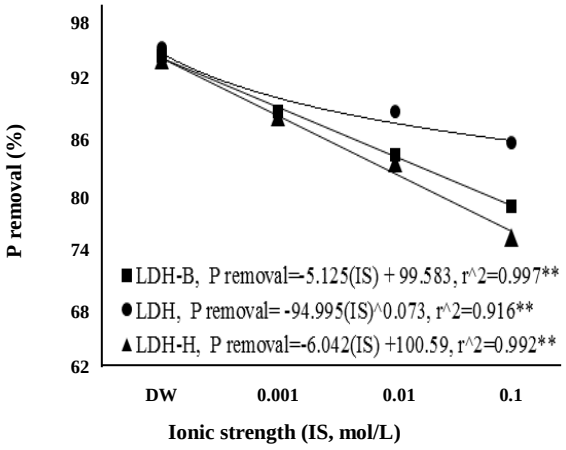

Fig. 7: Phosphate removal by LDH, LDH-biochar, and LDH-hydrochar under different concentrations of potassium chloride (P concentration = 50 mg/L, pH = 4, adsorbent dosage = 2 g/L at 22 °C).

of the solution ionic strength. The phosphate removal efficiency by the LDH, LDH-biochar and LDH-hydrochar at different levels of ionic strength could be predicted by regression equations presented in the Fig. 7.

The formation of surface complexes is pH dependent, but ion exchange is dependent on ionic strength [22]. Considering the effects of both pH and ionic strength on P adsorption on the LDH, LDH-biochar and LDH-hydrochar, it could be concluded that the formation of surface complexes and ion exchange are the main mechanisms of P adsorption by the studied adsorbents. Wan et al. [19] revealed that the predominant adsorption mechanisms of LDH-biochar were surface adsorption and interlayer ion exchange at low P concentrations, and precipitation of phosphate at high P concentrations. *Li et al.* [18] showed that combination of electrostatic attraction, anion exchange, and surface inner-sphere complex formation constituted the phosphate adsorption mechanisms of LDH-biochar.

Effect of adsorbent dosage

The effect of adsorbent dosage (solid-to-solution ratio) on phosphate adsorption by LDH, LDH-biochar, and LDH-hydrochar was shown in the Fig. 8. The phosphate removal rate (%) increased but the phosphate removal amount (mg/g) decreased with increasing adsorbent dosage (Fig. 8). All adsorbents that were examined removed more than about 97% of solution phosphate at an adsorbent dosage of 4 g/L (Fig. 8a), which was the optimum solid-to-solution ratio for adsorption of phosphate. The similar results have been reported by previous researchers [20,32].

Increasing phosphate removal with increasing solid-to-solution ratio is related to increasing active adsorption sites. Also, decreasing P removal with increasing solid-to-solution ratio is because of the fact that some adsorption sites remained unsaturated in high adsorbent levels [20].

The means comparison by t-test showed that there were no significant differences between P removal efficiency of the LDH, LDH-biochar and LDH-hydrochar irrespective of the adsorbent dosage. In addition, the exponential and polynomial equations were well fitted ($r^2>0.99^{**}$) to the data (Fig. 8a and b). So, these models can be used to predict the P removal efficiency and P adsorption at different adsorbent dosages and to achieve a given loading of phosphate by adsorbent in purification of wastewaters [19]. *Wan et al.* [19] reported the similar relationship ($r^2=0.986^{**}$) between equilibrium phosphate concentration and solid-to-solution ratio.

CONCLUSIONS

The Layered Double Hydroxide (LDH), LDH-biochar, and LDH-hydrochar composites were successfully prepared using the co-precipitation method. The SEM images revealed the deposition of the LDH particles on the biochar and hydrochar matrices. The adsorption of phosphate by the LDH, LDH-biochar, and LDH-hydrochar decreased with increasing the solution pH and ionic strength. The phosphate removal rate increased but the phosphate removal amount decreased with increasing the adsorbent dosage. The pseudo-second-order kinetic model was best fitted to the phosphate adsorption kinetics data. The LDH, LDH-biochar, and LDH-hydrochar exhibited rapid P adsorption, which reached equilibrium after about 30, 60, and 30 min, respectively. The maximum adsorption capacities of the LDH, LDH-biochar, and LDH-hydrochar calculated from the Langmuir model were 61.3, 55.6, and 51.7 mg P/g, respectively at the pH 4. However, the P removal efficiency of the LDH-biochar and LDH-hydrochar was similar to the LDH under different contact times, P concentrations, solution pH values, adsorbent dosages and ionic strengths. Considering all evidence, the present study could show that the phosphate adsorption on the LDH, LDH-biochar, and LDH-hydrochar was controlled

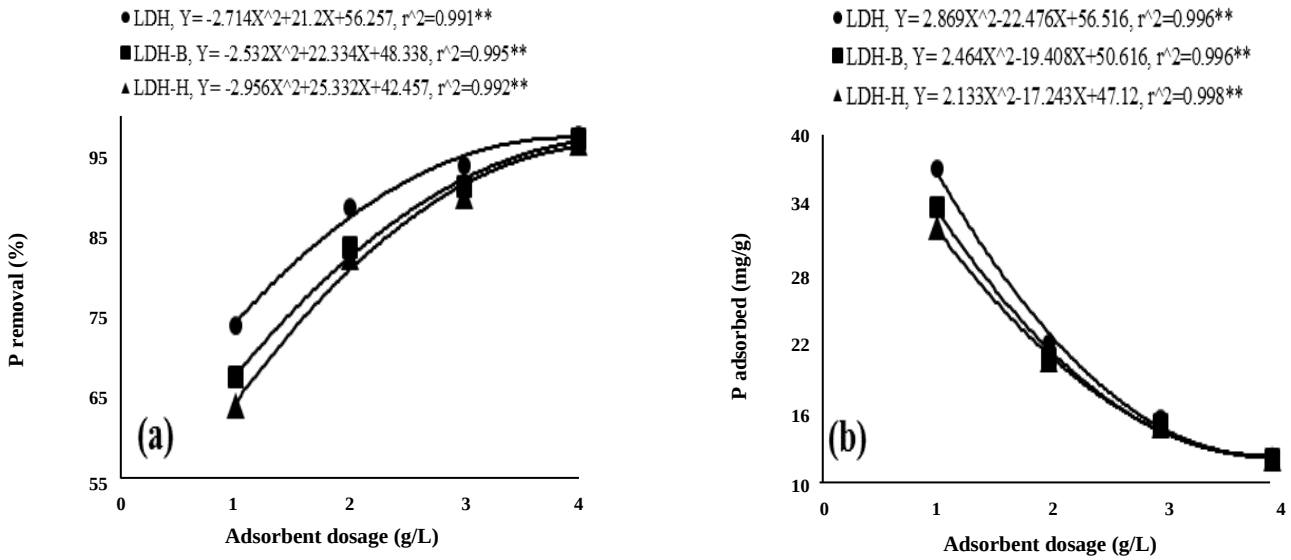

Fig. 8: Effect of LDH, LDH-biochar, and LDH-hydrochar dosage on removal (a), and P adsorption (b) (P concentration = 50 mg/L, pH = 4, I = 0.03 mol/L KCl at 22 ˚C).

by the surface electrostatic interaction, anion exchange, and surface inner-sphere complexation processes. The results confirmed that the LDH-biochar and LDH-hydrochar composites could be efficient and cost-effective adsorbents for the removal of phosphate from aqueous solutions. Also, the synthesized LDH-biochar and LDH-hydrochar composites have the potential use as P-fertilizers because of their high amount of P.

Acknowledgments

This paper is published as a part of a Ph.D. dissertation supported by the Vice-Chancellor for Research and Technology of the University of Tabriz, Iran. Authors are thankful to the University of Tabriz for their supports.

Received : Aug. 18, 2019 ; Accepted :Dec. 23, 2019

REFERENCES

[1] Desmidt E., Ghyselbrecht K., Zhang Y., Pinoy L., Van der Bruggen B., Verstraete W., Rabaey K., Meesschaert B., Global Phosphorus Scarcity and Full-scale P-recovery Techniques: A Review, *Crit. Rev. Env. Sci. Technol.*, **45**: 336-384 (2015).

[2] Lalley J., Han C., Li X., Dionysiou D.D., Nadagouda M.N., Phosphate Adsorption Using Modified Iron Oxide-based Adsorbents in Lake Water: Kinetics, Equilibrium, and Column Tests, *Chem. Eng. J.*, **284**: 1386-1396 (2016).

[3] Najafi N., "Phosphorus Slow Release Fertilizers: Preparation Methods and Their Effects on Phosphorus Uptake and Plant Growth", Presented at the *15th Iranian Soil Science Congress*, Isfahan, Iran, August 28-30. [In Persian with English Abstract] (2017).

[4] He H., Kang H., Ma S., Bai Y., Yang X., High Adsorption Selectivity of ZnAl Layered Double Hydroxides and the Calcined Materials Toward Phosphate, *J. Colloid Interface Sci.*, **343**: 225-231 (2010).

[5] Lǔ J., Liu H., Liu R., Zhao X., Sun L., Qu J., Adsorptive Removal of Phosphate by a Nanostructured Fe–Al–Mn Trimetal Oxide Adsorbent, *Powder Technol.*, **233**: 146-154 (2013).

[6] Yao Y., Gao B., Chen J., Yang L., Engineered Biochar Reclaiming Phosphate from Aqueous Solutions: Mechanisms and Potential Application as a Slow-Release Fertilizer, *Environ. Sci. Technol.*, **47**: 8700-8708 (2013a).

[7] Zhang M., Gao B., Fang J., Creamer A.E., Ullman J.L., Self-assembly of Needle-like Layered Double Hydroxide (LDH) Nanocrystals on Hydrochar: Characterization and Phosphate Removal Ability, *RSC Adv.*, **4**: 28171-28175 (2014).

[8] Khitous M., Salem Z., Halliche D., Removal of Phosphate from Industrial Wastewater Using Uncalcined MgAl-NO_3 Layered Double Hydroxide: Batch Study and Modeling, *Desalin. Water Treat.*, **57**: 15920-15931 (2016).

[9] Wang S., Gao B., Li Y., Zimmerman A.R., Cao X., Sorption of Arsenic Onto Ni/Fe Layered Double Hydroxide (LDH)-Biochar Composites, *RSC Adv.*, **6**: 17792-17799 (2016).

[10] Das J., Patra B., Baliarsingh N., Parida K., Adsorption of Phosphate by Layered Double Hydroxides in Aqueous Solutions, *Appl. Clay Sci.*, **32**: 252-260 (2006).

[11] Hosni K. Srasra E., Evaluation of Phosphate Removal from Water by Calcined-LDH Synthesized from the Dolomite, *Colloid J.*, **72**: 423-431 (2010).

[12] Li R., Wang J.J., Zhou B., Awasthi M.K., Ali A., Zhang Z., Lahori A.H., Mahar A., Recovery of Phosphate from Aqueous Solution by Magnesium Oxide Decorated Magnetic Biochar and its Potential as Phosphate-Based Fertilizer Substitute, *Bioresour. Technol.*, **215**: 209-214 (2016b).

[13] Goh K.H., Lim T.T., Dong Z., Removal of Arsenate from Aqueous Solution by Nanocrystalline Mg/Al Layered Double Hydroxide: Sorption Characteristics, Prospects, and Challenges, *Water Sci. Technol.*, **61**: 1411-1417 (2010b).

[14] Gokila B., Baskar K., Characterization of *Prosofis juliflora L*. Biochar and Its Influence of Soil Fertility on Maize in Alfisols, *Int. J. Plant Animal Environ. Sci*, **5**: 123-127 (2015).

[15] Xiao X., Chen B., Chen Z., Zhu L., Schnoor J.L., Insight Into Multiple and Multilevel Structures of Biochars and Their Potential Environmental Applications: A Critical Review, *Environ. Sci. Technol.*, **52(9)**: 5027-5047 (2018).

[16] Lian F., Xing B., Black Carbon (Biochar) in Water/Soil Environments: Molecular Structure, Sorption, Stability, and Potential Risk, *Environ. Sci. Technol.*, **51(23)**: 13517-13532 (2017).

[17] Zhang M., Gao B., Yao Y., Inyang M., Phosphate Removal Ability of Biochar/MgAl-LDH Ultra-Fine Composites Prepared by Liquid-Phase Deposition, *Chemosphere*, **92**: 1042-1047 (2013).

[18] Li R., Wang J.J., Zhou B., Awasthi M.K., Ali A., Zhang Z., Gaston L.A., Lahori A.H., Mahar A., Enhancing Phosphate Adsorption by Mg/Al Layered Double Hydroxide Functionalized Biochar with Different Mg/Al Ratios, *Sci. Total Environ.*, **559**: 121-129 (2016a).

[19] Wan S., Wang S., Li Y., Gao B., Functionalizing Biochar with Mg-Al and Mg–Fe Layered Double Hydroxides for Removal of Phosphate from Aqueous Solutions, *J. Indust. Eng. Chem.*, **47**: 246-253 (2017).

[20] Xue L., Gao B., Wan Y., Fang J., Wang S., Li Y., Muñoz-Carpena R., Yang L., High Efficiency and Selectivity of MgFe-LDH Modified Wheat-Straw Biochar in the Removal of Nitrate from Aqueous Solutions, *J. Taiwan Inst. Chem. Eng.*, **63**: 312-317 (2016).

[21] Tan X.-f., Liu Y.-g., Gu Y.-l., Liu S.-b., Zeng G.-m., Cai X., Hu X.-j., Wang H., Liu S.-m., Jiang L.-h., Biochar Pyrolyzed from MgAl-Layered Double Hydroxides Pre-coated Ramie Biomass (*Boehmeria nivea* (L.) Gaud.): Characterization and Application for Crystal Violet Removal, *J. Environ. Manage.*, **184**: 85-93 (2016).

[22] Zhao D., Feng S., Chen C., Chen S., Xu D., Wang X., Adsorption of Thorium (IV) on MX-80 Bentonite: Effect of pH, Ionic Strength and Temperature, *Appl. Clay Sci.*, **41**: 17-23 (2008).

[23] Li J., Hu J., Sheng G., Zhao G., Huang Q., Effect of pH, Ionic Strength, Foreign Ions and Temperature on the Adsorption of Cu (II) from Aqueous Solution to GMZ Bentonite, *Colloids Surf., A: Physicochemical and Engineering Aspects*, **349**: 195-201 (2009).

[24] Yao Y., Gao B., Inyang M., Zimmerman A.R., Cao X., Pullammanappallil P., Yang L., Removal of Phosphate from Aqueous Solution by Biochar Derived from Anaerobically Digested Sugar Beet Tailings, *J. Hazard. Mater.*, **190**: 501-507 (2011).

[25] Mohammadi M., Bahmanyar M., Sadeghzadeh F., Biparva P., Synthesis of Mg/Al Layered Double Hydroxide (LDH) Nanoplates for Efficient Removal of Nitrate from Aqueous Solutions, *J. Fundam. Appl. Sci*, **8**: 1058-1071 (2016).

[26] Ma W., Zhao N., Yang G., Tian L., Wang R., Removal of Fluoride Ions Fromaqueous Solution by the Calcination Product of Mg–Al–Fe Hydrotalcite-like Compound, *Desalination*, **268**(1): 20-26 (2011).

[27] Tran H.N., You S.J., Hosseini-Bandegharaei A., Chao H.P., Mistakes and Inconsistencies Regarding Adsorption of Contaminants from Aqueous Solutions: A Critical Review, *Water Res.*, **120**: 88-116 (2017).

[28] Ding L., Wu C., Deng H., Zhang X., Adsorptive Characteristics of Phosphate from Aqueous Solutions by MIEX Resin, *J. Colloid Interface Sci.*, **376(1)**: 224-232 (2012).

[29] Halajnia A., Oustan S., Najafi N., Khataee A., Lakzian A., The Adsorption Characteristics of Nitrate on Mg–Fe and Mg–Al Layered Double Hydroxides in a Simulated Soil Solution, *Appl. Clay Sci.*, **70**: 28-36 (2012).

[30] Hoseini S.R., Alidokht L., Oustan S., Aliasgharzad N., Najafi N., Kinetics of Cr(VI) Removal by Iron Filings in Some Soils, *Soil Sediment Contam.*, **24(5)**: 554-572 (2015).

[31] Evans D.G., Slade R.C., "Structural Aspects of Layered Double Hydroxides, Layered Double Hydroxides", Springer, pp. 1-87 (2006).

[32] Yan L.-g., Yang K., Shan R-r., Yan T., Wei J., Yu S.-j., Yu H.-q., Du B., Kinetic, Isotherm and Thermodynamic Investigations of Phosphate Adsorption Onto Core-Shell Fe3O4@LDHs Composites with Easy Magnetic Separation Assistance, *J. Colloid Interface Sci.*, **448**: 508-516 (2015).

[33] Zhou J., Yang S., Yu J., Shu Z., Novel Hollow Microspheres of Hierarchical Zinc–Aluminum Layered Double Hydroxides and Their Enhanced Adsorption Capacity for Phosphate in Water, *J. Hazard. Mater.*, **192(3)**: 1114-1121 (2011).

[34] Rives V., Kannan S., Layered Double Hydroxides with the Hydrotalcite-Type Structure Containing Cu^{2+}, Ni^{2+} and Al^{3+}, *J. Mater. Chem.*, **10**: 489-495 (2000).

[35] Goh K.H., Lim T.T., Banas A., Dong Z., Sorption Characteristics and Mechanisms of Oxyanions and Oxyhalides Having Different Molecular Properties on Mg/Al Layered Double Hydroxide Nanoparticles, *J. Hazard. Mater.*, **179**: 818-827 (2010a).

[36] Yao Y., Gao B., Chen J., Zhang M., Inyang M., Li Y., Alva A., Yang L., Engineered Carbon (Biochar) Prepared by Direct Pyrolysis of Mg-accumulated Tomato Tissues: Characterization and Phosphate Removal Potential, *Bioresour. Technol.*, **138**: 8-13 (2013b).

[37] Li R., Wang J.J., Zhou B., Zhang Z., Liu S., Lei S., Xiao R., Simultaneous Capture Removal of Phosphate, Ammonium and Organic Substances by MgO Impregnated Biochar and Its Potential Use in Swine Wastewater Treatment, *J. Clean. Prod.*, **147**: 96-107 (2017).

[38] Takaya C., Fletcher L., Singh S., Anyikude K., Ross A., Phosphate and Ammonium Sorption Capacity of Biochar and Hydrochar from Different Wastes, *Chemosphere*, **145**: 518-527 (2016).

[39] Seida Y., Nakano Y., Removal of Phosphate by Layered Double Hydroxides Containing Iron, *Water Res.*, **36**: 1306-1312 (2002).

[40] Fang C., Zhang T., Li P., Jiang R., Wu S., Nie H., Wang Y., Phosphorus Recovery from Biogas Fermentation Liquid by Ca–Mg Loaded Biochar, *J. Environ. Sci.*, **29**: 106-114 (2015).

[41] Krishnan K.A., Haridas A., Removal of Phosphate from Aqueous Solutions and Sewage Using Natural and Surface Modified Coir Pith, *J. Hazard. Mater.*, **152**: 527-535 (2008).

[42] Tajiki A., Abdouss M., Synthesis and Characterization of Graphene Oxide Nano-Sheets for Effective Removal of Copper Phthalocyanine from Aqueous Media, *Iran. J. Chem. Chem. Eng. (IJCCE)*, **36(4)**: 1-9 (2017).